ACS APPLIED MATERIALS & INTERFACES

Research Article

www.acsami.org

Silver Nanoparticles with an Armor Layer Embedded in the Alumina Matrix To Form Nanocermet Thin Films with Sound Thermal Stability

Junhua Gao, Chengjun Tu, Lingyan Liang, Hongliang Zhang, Fei Zhuge, Liang Wu, and Hongtao Cao*

Division of Functional Materials and Nano Devices, Ningbo Institute of Materials Technology & Engineering, Chinese Academy of Sciences, Ningbo 315201, People's Republic of China

Ke Yu

Royal Tech CSP Limited, Changzhou 213163, People's Republic of China

ABSTRACT: In this article, we demonstrate that the Al-alloyed Ag nanoparticle-embedded alumina nanocermet films lead to excellent thermal stability, even at 500 °C for 130 h under an ambient nitrogen atmosphere. The outward diffusion of Al atoms from the AgAl bimetallic alloy nanoparticles and their easy oxidation create an armor layer to suppress the mobility of Ag atoms. Then, the AlAg particles or/and agglomerates with a uniform spherical shape favor higher dispersion concentration within the host matrix, which is beneficial both for high absorptance in the visible range and for the solid localized surface plasmon absorption features in the AgAl−Al_2O_3 nanocermet films. Based on the AgAl−Al_2O_3 absorbing layer with sound optical and microstructural stability, we successfully constructed a high-temperature-endurable solar selective absorber. The multilayer stacked absorber demonstrates a high solar absorptance of ∼94.2% and a low thermal emittance of ∼15% (@ 673 K) after annealing at 450 °C for 70 h in an ambient nitrogen atmosphere.

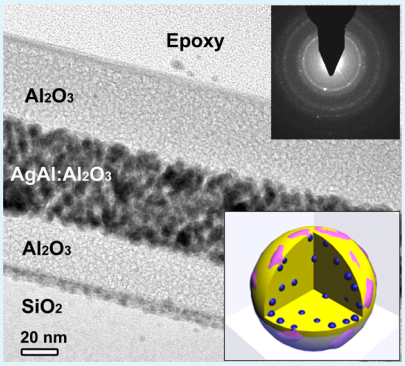

KEYWORDS: *silver nanoparticles, nanocermet thin films, thermal stability, diffusion, solar selective absorbing coating, bimetallic alloy*

1. INTRODUCTION

Because silver nanoparticles (AgNPs) possess outstanding absorption capacities in the visible regime and reasonable oxidation resistance at elevated temperatures, researchers have attempted to use them in the application of photothermal conversion.[1−3] In general, AgNPs are embedded into the ceramic host matrices (such as alumina) with a random distribution to form nanocermet materials, which have been utilized as the absorbing layer in the solar selective absorbing coatings.[1,2] Currently, silver nanoparticle/alumina (Ag−Al_2O_3) nanocermet films exhibit a promising candidate for high-temperature solar-selective absorbing coatings, because of their excellent optical properties and the favorable resistance to high-temperature oxidation. The solar absorptance as high as 93% is obtained only using a single Ag−Al_2O_3 composite layer.[1] The good absorbance is related to the plasmon resonance absorption effect of AgNPs in principle. This effect is sensitive to the size and shape of the nanoparticle, the configuration, and the surrounding medium.[4−7] Unfortunately, however, metal nanoparticles have an inherent tendency to agglomerate and grow, in order to minimize their surface energy under heating conditions. It has been found that the properties of Ag−Al_2O_3 nanocermet films evidently change at temperatures higher than 400 °C.[1,2] This phenomenon, as a key hurdle toward industrial applications, limits their use at high temperatures. Therefore, to address this issue, the thermal stability of AgNPs should be significantly enhanced. Alloying is an effective method to stabilize nanocrystalline structures at high temperatures.[8] Several bimetallic alloy nanoparticles, such as WTi,[8] PtNi,[9] AgAu,[10] etc., have been proven to be more stable than the pure metal counterparts under heating. The thermal stability improvement is ascribed to the segregation and occupation of the alloying atoms (solute) on the defective areas such as grain boundary and dislocation sites, which relaxes the low-coordinated surface and prevents the solvent atoms from rapid diffusion upon elevated temperatures. Therefore, in order to alloy AgNPs, the priority choice for the elements with low diffusion activation energy (E_a) in the bulk Ag is necessary. Al, as an effective dopant with low activation energy of 1.65 eV,[11] has played a role in refining the thermal endurance of Ag nanostructured films at 500 °C or even higher temperatures.[12,13] More importantly, the oxidation of the out-diffused Al atoms on the surface of the Ag particles or clusters to generate an armor layer, is efficient to form barriers resistant to Ag diffusion, which is undesirable.

In this paper, a AgAl−Al_2O_3 nanocermet film was proposed to inhibit diffusion, agglomeration, and coarsening of the embedded nanoparticles in the alumina matrix at high temperatures (>400 °C). With the addition of the Al atoms, it was believed that the reconstruction of the AgAl nano-

Received: April 14, 2014
Accepted: June 23, 2014
Published: June 23, 2014

Table 1. Deposition Parameters of Ag−Al_2O_3 and AgAl−Al_2O_3 Solar-Selective Absorbing Coatings

	Target Power (W)					
	Ag	Al	Al_2O_3	thickness (nm)	RF bias (W)	substrate rotating speed (rpm)
Al_2O_3 antireflection layer	0	0	120	∼58		
Ag−Al_2O_3 or AgAl−Al_2O_3 HMVF layer	8	0 or 8	120	∼53 or ∼79	0	
Ag−Al_2O_3 or AgAl−Al_2O_3 LMVF layer	10	0 or 10	120	∼20	35	20
Al_2O_3 diffusion barrier	0	0	120	∼30	0	
Ag or AgAl infrared reflector	39	0 or 20	0	∼160 or ∼100	0	

particles and the Al oxidation ease-generated armor layer under heating could be beneficial to prevent Ag atoms from migrating. As a result, the proposed nanocermet films possessing high tolerance to high temperatures could be obtained, which have numerous potential applications in harvesting solar thermal energy.

2. EXPERIMENTAL SECTION

Nanocermet films and solar selective absorbing coatings were deposited onto various substrates at room temperature by a multitarget sputtering system (Jsputter8000, manufactured by ULVAC Co., Ltd.). The commercially available high-purity Al_2O_3, Ag, and Al targets were used as the sputter sources. The location of these targets, 2 in. in diameter, is depicted in the form of a confocal configuration for co-sputtering preparation of nanocermet films. Prior to deposition, all the substrates were ultrasonically cleaned in acetone and alcohol baths for 15 min, then rinsed with deionized water, and finally dried under nitrogen flow. With a base pressure less than 2×10^{-4} Pa, all the deposition was implemented at a constant sputtering pressure of 0.22 Pa. Two radio-frequency (RF, 13.56 MHz) power supplies were used to operate the Al_2O_3 target and the Ag target, respectively, while the Al target was sputtered using a DC power source. Several single-layer Ag−Al_2O_3 or AgAl−Al_2O_3 films were deposited onto ultrathin carbon films supported by copper grid and Si(100) wafers for transmission electron microscopy (TEM) and scanning electron microscopy (SEM) analysis, respectively, with a deposition rate of 8.3 Å/min for Ag−Al_2O_3 and 9.5 Å/min for AgAl−Al_2O_3. The sputtering times for TEM and SEM samples were 5 and 17 min, respectively. For thermal stability analysis, a sandwich structure, comprising a Ag−Al_2O_3 or AgAl−Al_2O_3 layer between two alumina layers, was deposited onto silica slides. The sputtering power of the Ag, Al, and Al_2O_3 targets was 8, 0 or 8, and 120 W, respectively. As to the alumina layers, the deposition time was 50 and 60 min for the bottom and top layers with a thickness of ∼38 and 45 nm, respectively. Moreover, the sputtering time of Ag−Al_2O_3 or AgAl−Al_2O_3 nanocermet layers was 55 min.

Based on AgAl−Al_2O_3 composite films, high-temperature solar-selective absorbing coatings were prepared with the following structure: Al_2O_3(1)/double-nanocermet layer/Al_2O_3(2)/AgAl/SiO_2 substrate, in which Al_2O_3(1) and Al_2O_3(2) was selected as the antireflection and diffusion barrier layer, respectively. AgAl alloy film was deposited on the substrate directly, serving as the infrared reflector. The double-nanocermet layer was consisted of two AgAl−Al_2O_3 layers, one with a relatively low metal volume fraction (LMVF) onto the other with a higher metal volume fraction (HMVF). The deposition parameters for each layer are listed in Table 1. To compare with the AgAl−Al_2O_3 cases, Ag−Al_2O_3 solar-selective absorbing coatings were also prepared, as described in Table 1.

Preparation of the cross-sectional samples was carried out using mechanical thinning, followed by an ion milling or focused ion beam (FIB) method. The chemical composition of samples was investigated by X-ray photoelectron spectroscopy (XPS) analysis. The reflectance and transmittance of specimens were measured in the short wavelength ranging from 0.3 μm to 2.5 μm by the Lambda 950 spectrophotometer equipped with an integrating sphere. A Thermo Nicolet Model 6700 Fourier transform infrared (FTIR) spectrometer, with a Pike mid-infrared integrating sphere, was utilized to acquire the reflectance spectra in the infrared region (2.5−25 μm) at room temperature. The metal volume fraction of the nanocermet films was determined from fitting the ellipsometry spectra of the corresponding film deposited on Si(100) substrates. The heat treatment was performed in a tube furnace in an ambient or nitrogen atmosphere.

3. RESULTS AND DISCUSSION

3.1. Microstructure and Chemical Composition. In principle, the addition of the dopant would affect the microstructure characteristics of the nanoparticles, which governs their thermal stability.[14,15] Figure 1a and 1b shows the TEM images for the as-deposited Ag−Al_2O_3 and AgAl−Al_2O_3 nanocermet films, respectively. The volume fraction (f) of metal particles in the Ag−Al_2O_3 film is ∼40%. The majority of Ag nanoparticles, several nanometers in diameter and

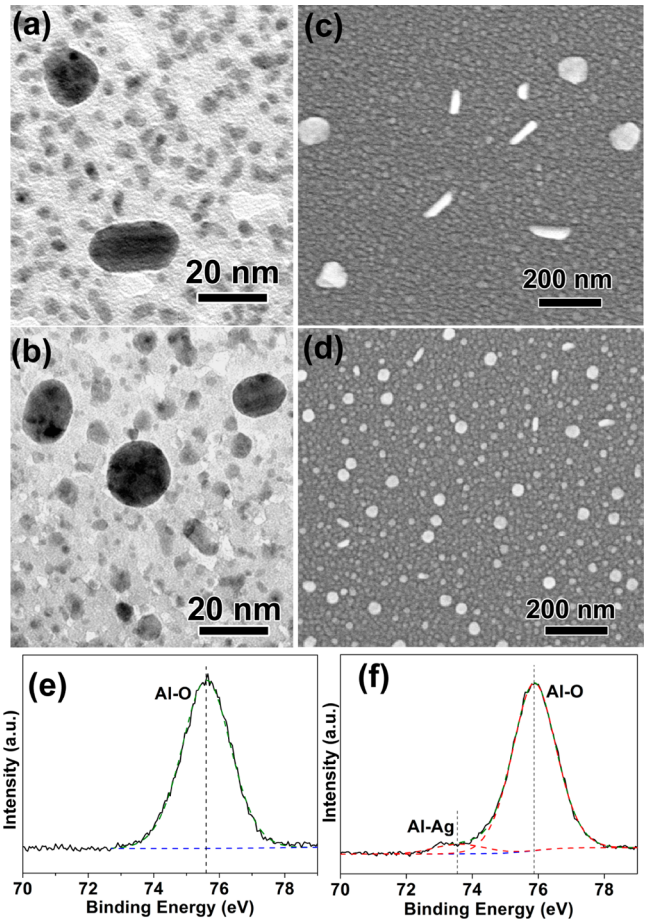

Figure 1. TEM images of (a) Ag−Al_2O_3 and (b) AgAl−Al_2O_3 cermet films with a deposition time of 5 min. SEM images of (c) Ag−Al_2O_3 and (d) AgAl−Al_2O_3 cermet films with a deposition time of 17 min. XPS spectra of Al 2p core levels for the (e) Ag−Al_2O_3 and (f) AgAl−Al_2O_3 samples with a deposition time of 60 min. The XPS spectra were obtained after Ar plasma etching for 240 s.

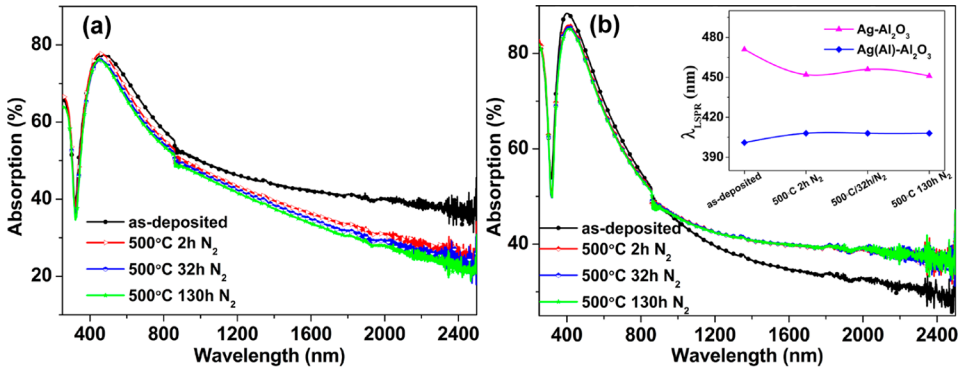

Figure 2. Light absorption spectra of the (a) Ag−Al_2O_3 and (b) AgAl−Al_2O_3 samples with different annealing durations. The two samples have a similar multilayer stacked structure, namely, consisting of a cermet layer between two alumina layers. The inset in panel b shows the evolution of the LSPR peak position (λ_{LSPR}) of the samples.

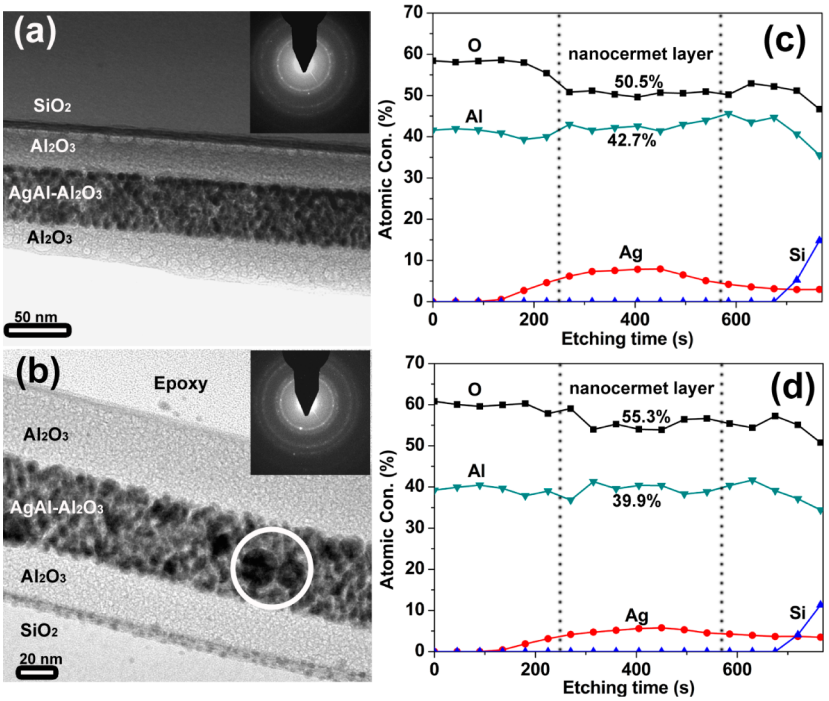

Figure 3. Cross-sectional TEM images of the samples shown in Figure 2b: (a) as-deposited and (b) annealed at 500 °C for 18 h; panels c and d give the corresponding XPS depth profiles before and after annealing, respectively. The insets show the corresponding SAED patterns of the nanocermet layers.

randomly distributed in the ceramic matrix, and a few Ag agglomerates or nanorods with larger size (even beyond 20 nm) were also observed, as seen in Figure 1a. Moreover, the dispersed AgNPs tend to aggregate, or be in tandem. With the addition of Al, however, the size of the agglomerates or nanorods decreased and the dispersion concentration of the agglomerates increased significantly, as verified by the TEM observation in Figure 1b, as well as the scanning electron microscopy (SEM) results in Figures 1c and 1d, indicating that the addition of Al into AgNPs has significant influence on the microstructure evolution. Furthermore, in comparison with Figure 1c, the agglomerates in Figure 1d, the features of which are near-spherical in shape, are more diffusely and homogeneously distributed throughout the alumina matrix. The metallic Al in the AgAl−Al_2O_3 film with a deposition time of 60 min was detected by X-ray photoelectron spectroscopy (XPS) after Ar plasma etching for 240 s. The metallic Al/Ag atomic ratio was calculated to be ∼1/9, so the AgAl−Al_2O_3 film was labeled as Ag(10 at.% Al)−Al_2O_3 cermet film. Compared to a single Al 2*p* core level peak in the Ag−Al_2O_3 film illustrated in Figure 1e, two Al 2*p* peaks, centered at 73.5 and 75.9 eV, were observed in the AgAl−Al_2O_3 film, as demonstrated in Figure 1f. It is reported that the binding energies of Al 2*p* core level peaks are near 73 and 76 eV for metallic Al and oxidation state of Al, respectively.[12] Combining the microstructure observation with the XPS analysis, it is speculated that the Al 2*p* peaks at 73.5 and 75.9 eV could be assigned to the AgAl alloy bonding and the Al−O bonding, respectively, further manifesting that the nanocermet film is consisted of both an AgAl alloy phase and an alumina phase. From either the AgAl bulk phase diagram or the related simulation point of view, the complete solid solution of Al in Ag is reliable in the concentration range employed in this study.[16,17] Furthermore, the related computational simulation manifests that the alloyed nanoparticles have more negative formation energy than the core−shell nanoparticles, meaning that the former is more stable than the latter,

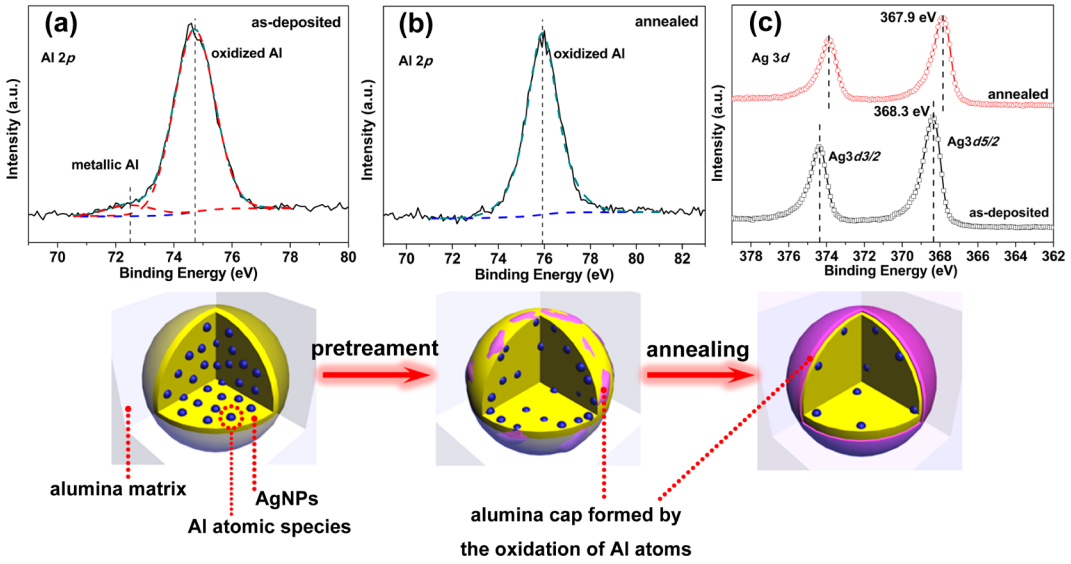

Figure 4. Al 2*p* core level spectra of the AgAl−Al_2O_3 cases shown in Figure 3: (a) as-deposited and (b) annealed at 500 °C for 18 h. Panel c presents the Ag 3*d* core level spectra of the samples before and after annealing. The spectra were recorded after Ar plasma etching for 405 s. Bottom portions of Figure 4 give schematic illustrations of the microstructure evolution of the AgAl nanoparticle in AgAl−Al_2O_3 cermet films, which were pretreated at 200 and 300 °C, in turn, in air for 2 h, and then annealed at 500 °C in an ambient nitrogen atmosphere.

especially for the particles with several nanometers in diameter.[10,18]

3.2. Thermal Stability Analysis. The Al_2O_3/Ag−Al_2O_3/Al_2O_3 and Al_2O_3/Ag(10 at.% Al)−Al_2O_3/Al_2O_3 sandwich structures were first pretreated, in turn, at 200 and 300 °C in air for 2 h. Then, the optical properties were investigated as a function of the annealing duration time (500 °C in an ambient nitrogen atmosphere). It should be noted that the top and bottom alumina layers in the sandwich structure were applied to avoid the environmental or substrate effects. Figures 2a and 2b exhibit the optical absorption, ranging from 300 nm to 2500 nm for the Ag−Al_2O_3 and Ag(10 at.% Al)−Al_2O_3 films, respectively. The reflectance and transmittance curves were first recorded using a Lambda 950 UV/vis/NIR spectrophotometer. Then, since the sum of absorbance $A(\lambda)$, reflectance $R(\lambda)$, and transmittance $T(\lambda)$ at each wavelength λ must be equal to unity, the absorbance could be derived as $A(\lambda) = 1 - R(\lambda) - T(\lambda)$. For the Ag−$Al_2O_3$ case, the localized surface plasmon absorption (LSPR) band at ∼471 nm was observed to have a blue-shift after the heat treatment. Meanwhile, the absorbance intensity decreased to some extent in the entire measurement range, especially at $\lambda > 450$ nm. In contrast, the AgAl−Al_2O_3 film did not show any significant variation of the LSPR peak position (∼405 nm), and its absorbance was enhanced in the long wavelength range (>950 nm), as compared to a negligible decrease in the short wavelength region. The inset to Figure 2b depicts the evolution of the LSPR peak position (λ_{LSPR}) with the heat-treatment duration. To summarize the optical property analysis presented in Figure 2, one can envisage that the introduction of Al into the Ag−Al_2O_3, which gives rise to the alloying of the Ag nanoparticles, is favorable to stabilize the so-called localized surface plasmon absorption phenomena. It is known that the position of the LSPR peak and the peak intensity is sensitively influenced by the microstructure characteristics (including size, shape, or configuration) of the AgNPs. The metal nanoparticles with a near spherical shape is usually more stable than the isolated nanoparticles with random shapes under heating conditions, since the former has lower surface free energy.[14,19] Therefore, the population density increase of the Ag agglomerates and the particle-shape constancy caused by the alloying agent of Al, as manifested in Figure 1, could be partially account for the stable LSPR features for the AgAl−Al_2O_3 films.

The optical stability is essentially coupled with the microstructural stability of the AgAl−Al_2O_3 films, confirmed by the cross-sectional TEM observations in Figure 3. Figure 3a clearly shows the sandwich structure of the as-deposited specimen. In particular, the nanocermet layer is consisted of the randomly distributed AgAl nanocrystals and the amorphous matrix, as evidenced by the TEM images and the selective area electron diffraction (SAED) patterns (as shown in the inset). After heat treatment at 500 °C for 18 h in a nitrogen atmosphere (the preannealing procedure is the same as the samples in Figure 2), the well-defined interfaces between different layers are distinguishable, as illustrated in Figure 3b. The thickness of the nanocermet layer is kept at ∼50 nm. It is believed that the microstructural feature of the nanocermet layer was maintained after heat treatment, although the agglomeration behavior of the nanoparticles was present via Ostwald ripening process (as marked using a white circle in Figure 3b). The compositional depth profile is exhibited in Figures 3c and 3d, which is corresponding to the as-deposited sample and the annealed one, respectively. Compared to the as-deposited case, the average oxygen concentration was increased from 50.5 at. % to 55.3 at. % in the annealed sample, accompanying a slight content reduction for elemental Al and Ag. It should be pointed out that the distribution profile of Ag within the nanocermet layer does not show any obvious variation before and after annealing, except for the relative concentration. Meanwhile, no distinguishable silver diffusate was detected in the alumina protective layer. Therefore, it can be deduced that the inward diffusion of oxygen into the nanocermet inner layer is present. In addition, the distribution profile variation of Al throughout the nanocermet layer suggested its rearrangement in the ceramic matrix.

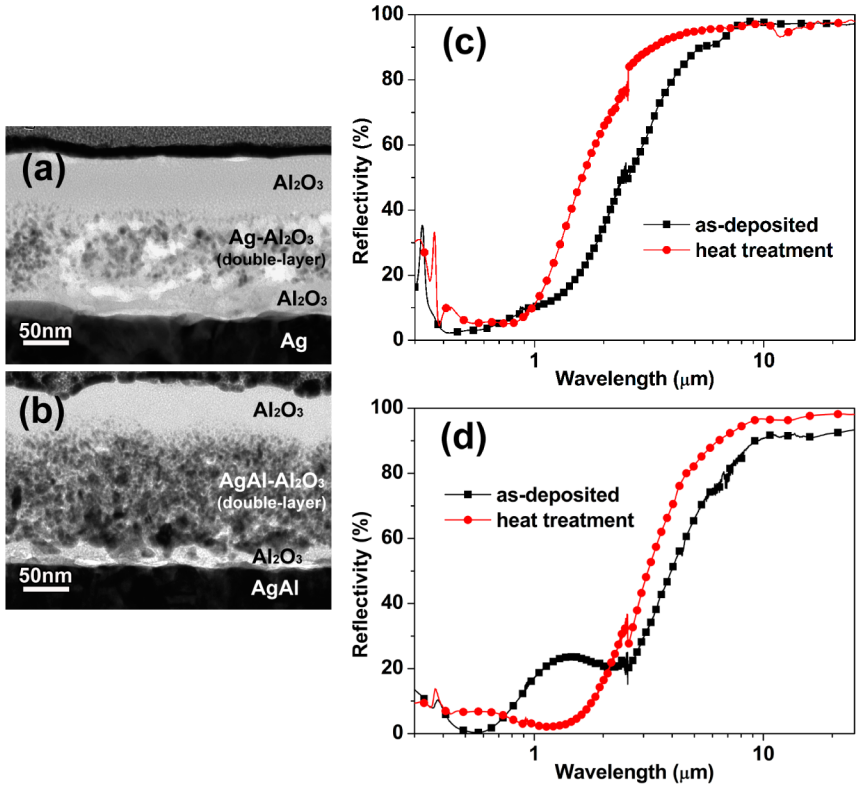

Figure 5. Cross-sectional TEM images of the (a) Ag–Al_2O_3 and (b) AgAl–Al_2O_3 solar absorbing coatings annealed at 450 °C for 70 h in an ambient nitrogen atmosphere. Comparisons of the reflectance spectra between the as-deposited and the annealed coatings for the Ag–Al_2O_3 and AgAl–Al_2O_3 are shown in panels c and d, respectively.

Figure 4 shows the binding energies for Al 2*p* and Ag 3*d* core level peaks of the AgAl–Al_2O_3 film before and after annealing at 500 °C for 18 h. The XPS measurement was recorded after etching the samples for 405 s. The peak centered at the 72.5 and 74.9 eV is corresponding to the metallic Al and the oxidized Al, respectively, as depicted in Figure 4a. In contrast, there is only a single peak at 75.8 eV (in Figure 4b) after annealing, which is allocated to the oxidation state of Al. In theory, the formation of the Al–O bonding is more preferential than that of Ag–O bonding, because the Gibbs energy of formation of Al_2O_3 and Ag_2O at 500 °C is −1433 kJ/mol and >2.06 kJ/mol,[20] respectively. Hence, it is expected that the oxidation of metallic Al, instead of metallic Ag, easily occurs in the ceramic matrix, which is verified by the fact that there is negligible variation before and after annealing concerning whether the Ag 3*d* peak position shift or Ag 3*d* peak shape, as presented in Figure 4c. Based on the above XPS analysis, it is proposed that the metallic Al diffused out of the AgAl nanoparticles, and got oxidized preferentially to form an armor layer to suppress the outward diffusion of Ag into the ceramic host.

The investigation on thermal diffusion between Al and Al_2O_3 thin films uncovered that the mutual interdiffusion phenomenon that occurred in the interface region dominated over the compositional change in the Al_2O_3/Al/glass system at low temperatures (from 200 °C to 400 °C).[21] More specifically, the metallic Al had diffused into the Al_2O_3 layer with simultaneous diffusion of the oxygen into the Al layer, indicating that the diffused Al atoms are prone to be oxidized when encountering the Al_2O_3 layer. Moreover, it is well-known that there are some microcracks or narrow channels (e.g., holes, voids or grain boundaries) within the sputtered films deposited at room temperature. These defects can provide rapid paths for diffusion. In this study, oxygen from surrounding environment can diffuse through the alumina layer and then react with the metal particles in the cermet layer when annealing at relatively high temperatures, as reported elsewhere.[22,23] Based on the previous report, as well as the results revealed in Figures 2, 3, and 4, one can figure out the mechanism to interpret the optical and microstructural stability of the AgAl–Al_2O_3 nanocermet, as schematically illustrated in the bottom of Figure 4. During the low-temperature pretreatment in air, the Al atoms in the AgAl alloy nanoparticles mainly tend to occupy the interfacial sites between the particles and the alumina matrix, and then get oxidized near the interface. This behavior is consistent with the previous studies on oxidation-driven restructuring of bimetallic nanoparticles,[24] namely, that the better stability of alumina compared to silver oxide provides the driving force for the preferential oxidation of Al and oxide-phase segregation at the particle/matrix interfaces. Thus, the easily generated oxide phase, acting as the armor layer partially covering the sphere of the alloy nanoparticles, could boost the diffusion barrier to prohibit the outward diffusion of Ag. It should be emphasized that the freshly generated alumina (quite different from the already existed alumina host) riveted on the AgAl particle surface might has strong chemical bonding, which is supported by the fact that the dewetting phenomenon is absent at the interface between the AgAl film and the SiO_2 substrate.[25] The alumina armor layer is analogy to the surfactant in microemulsions, which is just used to stabilize interfacial area.[26] It is noteworthy that the oxidation of Al to form alumina armor layer would not obviously modify the dielectric functions of the nanocermet layer, and thus is favorable for the stability of the LSPR absorption shown in Figure 2b. In addition, this AgAl

nanoparticle surface oxidation also led to the obvious increase of absorption in the infrared region, as presented in Figure 2b. The decreased reflectance as well as the increased absorbance in the infrared region is achieved at the expense of metallic Al loss under annealing. From the above discussion, it is believed that the oxidation of the dopant Al and the armor layer formation would play a critical role in maintaining the LSPR signal (Figure 2) and microstructure stability (Figure 3) of the cermet layer at high temperatures (>400 °C). Unfortunately, because of the limited Al dopant concentration and the present of elemental Al both in the alloy particles and the matrix phase, it was difficult to visually observe the oxidation behavior of Al on the particle surface and the oxide phase segregation.

3.3. Solar-Selective Absorbing Coatings and Their Thermal Stability. High-temperature solar-selective absorbing coatings were designed and fabricated with the following structure: Al_2O_3/double-nanocermet layer/Al_2O_3/AgAl/SiO_2 substrate. In comparison with pure Ag film, AgAl alloy film, serving as the infrared reflector, possesses higher thermal endurance.[12,13] Also, the alloy film with high electrical conductivity is in favor of keeping high reflectance in the infrared region. Generally, the optimized double-nanocermet layer consists of a LMVF nanocermet layer on a HMVF section, in order to efficiently harvest the solar light by means of both absorption and the interference effect.[27] The volume fraction (f) of AgAl particles in the HMVF and LMVF layer is ∼40% and ∼15%, respectively, which was obtained by fitting the ellipsometry spectra of the respective single nanocermet film deposited on Si(100) substrates. The fitting was performed using a quasi-static approach, in which the Maxwell Garnett model and the Bruggeman model is applicable for LMVF and HMVF layer, respectively.[28] Moreover, the averaged Al percentage in the AgAl nanoparticles of the LMVF, HMVF nanocermet, and AgAl infrared reflector layer is 10, 15, and 6 at. %, respectively. An absorbing coating with a Al_2O_3/Ag−Al_2O_3(LMVF)/Ag−Al_2O_3(HMVF)/Al_2O_3/Ag/SiO_2 structure was also prepared as a control. The sputtering parameters for the two types of absorbing coatings are similar, except for the Al doping in the double-nanocermet layer and the infrared reflector (see Table 1). After the same preannealing procedure as the specimen shown in Figures 2 and 3, the above absorbing coatings were sequentially annealed at 450 °C for 70 h in a nitrogen atmosphere. The cross-sectional TEM observations are shown in Figures 5a and 5b, in order to investigate their structural stability at elevated temperatures. For the Ag−Al_2O_3 case, the double-nanocermet layer had become porous and the interface between the two nanocermet layers was not clear, because of serious agglomeration of the particles and their outward diffusion. The degradation trend of the Ag−Al_2O_3 nanocermet layer is consistent with the behavior reported elsewhere.[2] In contrast, however, the AgAl−Al_2O_3 absorbing coating was observed to keep its structural integrity with a sharp interface, as shown in Figure 5b. It should be emphasized that the interface region between the metal infrared reflector and the alumina barrier layer is smooth and well-defined in the AgAl−Al_2O_3 absorbing coating, as respectively illustrated in Figures 5b and 5a. This further confirmed that the addition of Al into Ag nanoparticles is capable of promoting the microstructure stability.

Figures 5c and 5d display the reflectance of the two types of absorbing coatings before and after annealing, respectively. A low reflection within the solar spectral regime (0.3−2.5 μm) is desirable for obtaining high solar absorptance, while a high reflection in the infrared region (>2.5 μm) implies low thermal loss. In comparison with the as-deposited Ag−Al_2O_3 absorbing coating, it is found that the reflectance of the Ag−Al_2O_3 absorbing coating after heat treatment has increased in the entire measurement range, meaning that the absorption ability of the Ag−Al_2O_3 absorbing coating in the solar spectrum region (0.3−2.5 μm) has degraded significantly with the temperature. Nevertheless, for the AgAl−Al_2O_3 case, the overall reflectance of the annealed coating in the solar spectrum region is beneficially reduced, while its reflection in the infrared range is upgraded desirably, which leads to the improvement of the spectral selectivity of the absorbing coating.[27] Two important parameters, solar absorptance α and thermal emittance ε, can be derived from the reflectance spectrum, which is defined as[29]

$$\alpha = \frac{\int_{0.3\,\mu m}^{2.5\,\mu m} I_{sol}(\lambda)[1 - R(\lambda)]\,d\lambda}{\int_{0.3\,\mu m}^{2.5\,\mu m} I_{sol}(\lambda)\,d\lambda} \quad (1a)$$

$$\varepsilon = \frac{\int_{2.5\,\mu m}^{25\,\mu m} I_{p}(\lambda)[1 - R(\lambda)]\,d\lambda}{\int_{2.5\,\mu m}^{25\,\mu m} I_{p}(\lambda)\,d\lambda} \quad (1b)$$

where $I_{sol}(\lambda)$ is the radiation intensity in air mass (AM) 1.5 sunlight, $I_p(\lambda)$ the radiation intensity in the blackbody radiation spectrum at a certain temperature, and $R(\lambda)$ the spectral reflectance. Specifically, the absorption α and the emissivity ε of the selective absorbing coating reflect the ability to harvest the solar energy and to dissipate thermal energy in the infrared regime, respectively. Therefore, the coating for solar thermal applications simultaneously possesses high absorption α in the solar spectrum and low infrared emissivity. For the as-deposited cases, the absorptance α and the emissivity ε (at 673 K) are 91% and 11.7% for the Ag−Al_2O_3 absorbing coating and 89% and 33% for the AgAl−Al_2O_3 one, respectively. After annealing at 450 °C for 70 h, however, the absorptance α of the Ag−Al_2O_3 sample drastically dropped to 84%, while that of the AgAl−Al_2O_3 specimen significantly increased to 94.2%. Evidently, the serious absorptance degradation of the Ag−Al_2O_3 absorbing coating is unsatisfying for high-temperature applications. Based upon the LSPR and TEM observations, the overall optical degradation of absorbing coating stemmed from the collapse of the LSPR characteristics, as well as the adverse microstructure evolution in the cermet layers. Also, the interfacial structure evolution in the stacked multilayers cannot be ruled out to account for the performance degradation. Interestingly, the emissivity (ε) of the AgAl−Al_2O_3 absorbing coating does present a significant reduction, i.e., from 33% (as-deposited) to 15.4% (annealed). The optical performance of the annealed AgAl−Al_2O_3 absorbing coating is comparable to the previous report using Mo-SiO_2 cermet as the absorbing layer.[30] It is well-known that metal element diffusion and oxidation generally caused the performance failure of the solar absorber under the thermal aging conditions.[27] In our study, however, we make full use of the element diffusion and oxidation by introducing metallic Al into Ag nanoparticles to form alloyed AgAl nanoparticles. After pretreatment in air, Al atoms, serving as "sacrificial" matter, are so active that they diffuse out of the alloy particles easily, then preferentially react with the residual oxygen to develop local oxidation layer (Gibbs free energy of alumina is more negative than that of Ag-related oxides). Although locally situated on the sphere of the AgAl nanoparcicles, the easily generated oxide layer, serving as the

armor layer, is capable of inhibiting the outdiffusion of Ag atoms, stabilizing the LSPR features, and maintaining the microstructure changes as little as possible. The alloy AgAl nanoparticle embedded alumina is used as the absorbing nanocermet layer to construct the entire multilayer stacked absorbing coating, eventually leading to the promotion of the optical performance and the thermal stability as well.

Because the optical constants (refractive index and extinction coefficient) are sensitive to the composition and the microstructure changes of the nanocermet materials, optical properties of solar selective absorbing coatings are, hence, subject to change, because of the thermal diffusion and/or oxidation of the embedded particles.[31] Thus, the performance of the entire AgAl−Al_2O_3 solar-selective absorbing coating can be further optimized by finely tailoring both the amount of the dopant of Al and the thickness of each layer; this research is currently underway in our group.

4. CONCLUSION

In summary, we investigated the effect of AgAl bimetallic alloy nanoparticle on the thermal diffusion of Ag atoms in the nanocermet films. The thermal stability of AgAl−Al_2O_3 films is significantly improved by the oxidation and rearrangement of Al, rather than the improvement of the melting point of AgAl particles, which is quite different from the conventional nanocermet materials consisting of high-melting-point metal or alloy nanoparticles dispersed in refractory ceramic matrixes (e.g., Mo−Al_2O_3 and NiAl−Al_2O_3). Based on the AgAl−Al_2O_3 absorbing layer, a solar-selective absorbing coating with a high solar absorptance ∼94.2% and a low thermal emittance ∼15% (at 673 K) was obtained after annealing at 450 °C in a nitrogen ambient for 70 h. These results demonstrate that the proposed AgAl−Al_2O_3 material has great potential for high-temperature solar thermal applications.

AUTHOR INFORMATION

Corresponding Author

*Tel.: +86 (0)574 86685161. E-mail: h_cao@nimte.ac.cn.

Notes

The authors declare no competing financial interest.

ACKNOWLEDGMENTS

We acknowledge the financial support from the National Nature Science Foundation of China (Grant No. 51302277), the Ningbo Nature Science Foundation (Grant No. 2013A610073) and the Project funded by China Postdoctoral Science Foundation.

REFERENCES

(1) Barshilia, H. C.; Kumar, P.; Rajam, K. S.; Biswas, A. Structure and Optical Properties of Ag-Al_2O_3 Nanocermet Solar Selective Coatings Prepared Using Unbalanced Magnetron Sputtering. *Sol. Energy Mater. Sol. Cells* **2011**, *95*, 1707−1715.

(2) Xiao, X. D.; Xu, G.; Xiong, B.; Chen, D. M.; Miao, L. The Film Thickness Dependent Thermal Stability of Al_2O_3:Ag Thin Films as High-Temperature Solar Selective Absorbers. *J. Nanopart. Res.* **2012**, *14*, 746.

(3) Gao, T.; Jelle, B. P.; Gustavsen, A. Core-Shell-Typed Ag@SiO_2 Nanoparticles as Solar Selective Coating Materials. *J. Nanopart. Res.* **2013**, *15*, 1370.

(4) Mandal, S. K.; Roy, R. K.; Pal, A. K. Surface Plasmon Resonance in Nanocrystalline Silver Particles Embedded in SiO_2 Matrix. *J. Phys. D: Appl. Phys.* **2002**, *35*, 2198−2205.

(5) Kelly, K. L.; Coronado, E.; Zhao, L. L.; Schatz, G. C. The Optical Properties of Metal Nanoparticles: The Influence of Size, Shape, and Dielectric Environment. *J. Phys. Chem. B* **2003**, *107*, 668−677.

(6) Lermé, J.; Palpant, B.; Prével, B.; Pellarin, M.; Treilleux, M.; Vialle, J. L.; Perez, A.; Broyer, M. Quenching of the Size Effects in Free and Matrix-Embedded Silver Clusters. *Phys. Rev. Lett.* **1998**, *80*, 5105−5108.

(7) Langille, M. R.; Personick, M. L.; Mirkin, C. Plasmon-Mediated Syntheses of Metallic Nanostructures. *Angew. Chem., Int. Ed.* **2013**, *52*, 13910−13940.

(8) Chookajorn, T.; Murdoch, H. A.; Schuh, C. A. Design of Stable Nanocrystalline Alloys. *Science* **2012**, *337*, 951−954.

(9) Cui, C. H.; Gan, L.; Heggen, M.; Rudi, S.; Strasser, P. Compositional Segregation in Shaped Pt Alloy Nanoparticles and Their Structural Behavior During Electrocatalysis. *Nat. Mater.* **2013**, *12*, 765−771.

(10) Li, Y.; Qi, W. H.; Huang, B. Y.; Ji, W. H.; Wang, M. P. Size- and Composition-Dependent Structural Stability of Core−Shell and Alloy Pd-Pt and Au-Ag Nanoparticles. *J. Phys. Chem. C* **2013**, *117*, 15394−15401.

(11) Wang, Y.; Alford, T. L. Formation of Aluminum Oxynitride Diffusion Barriers for Ag Metallization. *Appl. Phys. Lett.* **1999**, *74*, 52−54.

(12) Kim, J. Y.; Na, S. I.; Ha, G. Y.; Kwon, M. K.; Park, I. K.; Lim, J. H.; Park, S. J. Thermally Stable and Highly Reflective AgAl Alloy for Enhancing Light Extraction Efficiency in GaN Light-Emitting Diodes. *Appl. Phys. Lett.* **2006**, *88*, 043507.

(13) Kim, H. C.; Theodore, N. D.; Mayer, J. W.; Alford, T. L. Thermal Stability and Electrical Properties of Ag(Al) Metallization. *Mater. Res. Soc. Symp. Proc.* **2004**, *812* (F3.24), 1−6.

(14) Sengar, S. K.; Mehta, B. R.; Govind. Size and Alloying Induced Changes in Lattice Constant, Core, and Valance Band Binding Energy in Pd-Ag, Pd, and Ag Nanoparticles: Effect of In-Flight Sintering Temperature. *J. Appl. Phys.* **2012**, *112*, 014307.

(15) Zhang, Z. Y.; Nenoff, T. M.; Leung, K.; Ferreira, S. R.; Huang, J. Y.; Berry, D. T.; Provencio, P. P.; Stumpf, R. Room-Temperature Synthesis of Ag-Ni and Pd-Ni Alloy Nanoparticles. *J. Phys. Chem. C* **2010**, *114*, 14309−14318.

(16) Zarkevich, N. Z.; Johnson, D. D. Predicted hcp Ag-Al Metastable Phase Diagram, Equilibrium Ground States, and Precipitate Structure. *Phys. Rev. B* **2003**, *67*, 064104.

(17) Asta, M.; Hoyt, J. J. Thermodynamic Properties of Coherent Interfaces in F.C.C.-Based Ag-Al Alloys: A First-Principles Study. *Acta Mater.* **2000**, *48*, 1089−1096.

(18) Qi, W. H.; Lee, S. T. Phase Stability, Melting, and Alloy Formation of Au-Ag Bimetallic Nanoparticles. *J. Phys. Chem. C* **2010**, *114*, 9580−9587.

(19) Li, J.; Lin, Y. Q.; Zhao, B. G. Spontaneous Agglomeration of Silver Nanoparticles Deposited on Carbon Film Surface. *J. Nanopart. Res.* **2002**, *4*, 345−349.

(20) Barin, I. I.; Platzki, G. *Thermochemical Data of Pure Substances*, 3rd Edition; VCH Verlagsgesellschaft mbH: Weinheim, Germany, 1995.

(21) García-Méndez, M.; V.alles-Villarreal, N.; Hirata-Flores, G. A.; Farías, M. H. Study of Thermal Diffusion between Al_2O_3 and Al Thin Films. *Appl. Surf. Sci.* **1999**, *151*, 139−147.

(22) Gatt, R.; Niklasson, G. A.; Granqvist, C. G. Degradation Modes of Cermet Based Selectively Solar Absorbing Coatings. *Proc. SPIE France* **1992**, *1727*, 87−101.

(23) Selvakumar, N.; Manikandanath, N. T.; Biswas, A.; Barshilia, H. C. Design and Fabrication of Highly Thermally Stable HfMoN/HfON/Al_2O_3 Tandem Absorber for Solar Thermal Power Generation Applications. *Sol. Energy Mater. Sol. Cells* **2012**, *102*, 86−92.

(24) Tao, F.; Grass, M. E.; Zhang, Y. W.; Butcher, D. R.; Renzas, J. R.; Liu, Z.; Chung, J. Y.; Mun, B. S.; Salmeron, M.; Somorjai, G. A. Reaction-Driven Restructuring of Rh-Pd and Pt-Pd Core−Shell Nanoparticles. *Science* **2008**, *322*, 932−934.

(25) Sugawara, K.; Minamide, Y.; Kawamura, M.; Abe, Y.; Sasaki, K. Agglomeration Behaviour of Ag Films Suppressed by Alloying with Some Elements. *Vacuum* **2009**, *83*, 610−613.
(26) Kahlweit, M. Microemulsions. *Science* **1988**, *240*, 617−621.
(27) Selvakumar, N.; Barshilia, H. C. Review of Physical Vapor Deposited (PVD) Spectrally Selective Coatings for Mid- and High-Temperature Solar Thermal Applications. *Sol. Energy Mater. Sol. Cells* **2012**, *98*, 1−23.
(28) Nejati, M. R.; Fathollahi, V.; Asadi, M. K. Computer Simulation of The Optical Properties of High-Temperature Cermet Solar Selective Coatings. *Sol. Energy* **2005**, *78*, 235−241.
(29) Wang, X. X.; Li, H. F.; Yu, X. B.; Shi, X. L.; Liu, J. F. High-Performance Solution-Processed Plasmonic Ni Nanochain-Al_2O_3 Selective Solar Thermal Absorber. *Appl. Phys. Lett.* **2012**, *101*, 203109.
(30) Esposito, S.; Antonaia, A.; Addonizio, M. L.; Aprea, S. Fabrication and Optimisation of Highly Efficient Cermet-Based Spectrally Selective Coatings for High Operating Temperature. *Thin Solid Films* **2009**, *517*, 6000−6006.
(31) Cheng, J. S.; Wang, C.; Wang, W. W.; Du, X. K.; Liu, Y.; Xue, Y. F.; Wang, T. M.; Chen, B. L. Improvement of the Thermal Stability in the Solar Selective Absorbing Mo-Al_2O_3 Coating. *Sol. Energy Mater. Sol. Cells* **2013**, *109*, 204−208.